Evaluation of a Statistical Model of Cloud Vertical Structure Using Combined *CloudSat* and CALIPSO Cloud Layer Profiles

WILLIAM B. ROSSOW

CREST at The City College of New York, New York, New York

YUANCHONG ZHANG

Department of Applied Physics and Applied Mathematics, Columbia University, and NASA Goddard Institute for Space Studies, New York, New York

(Manuscript received 17 March 2010, in final form 11 August 2010)

ABSTRACT

A model of the three-dimensional distribution of clouds was developed from the statistics of cloud layer occurrence from the International Satellite Cloud Climatology Project (ISCCP) and the statistics of cloud vertical structure (CVS) from an analysis of radiosonde humidity profiles. The CVS model associates each cloud type, defined by cloud-top pressure of the topmost cloud layer and total column optical thickness, with a particular CVS. The advent of satellite cloud radar (*CloudSat*) and lidar [Cloud–Aerosol Lidar and Infrared Pathfinder Satellite Observations (CALIPSO)] measurements (together C&C) of CVS allows for a quantitative evaluation of this statistical model. The zonal monthly-mean cloud layer distribution from the ISCCP CVS agrees with that from C&C to within 10% (when normalized to the same total cloud amount). The largest differences are an overestimate of middle-level cloudiness in winter polar regions, an overestimate of cloud-top pressures of the highest-level clouds, especially in the tropics, and an underestimate of low-level cloud amounts over southern midlatitude oceans. A more severe test of the hypothesized relationship is made by comparing CVS for individual satellite pixels. The agreement of CVS is good for isolated low-level clouds and reasonably good when the uppermost cloud layer is a high-level cloud; however, the agreement is not good when the uppermost cloud layer is a middle-level cloud, even when ISCCP correctly locates cloud top. An improved CVS model combining C&C and ISCCP may require classification at spatial scales larger than individual satellite pixels.

1. Introduction

The effect of clouds on the atmospheric motions that produce them is determined by the vertical and horizontal gradients of diabatic heating (e.g., Rind and Rossow 1984) by both the precipitation formed in clouds and the radiative flux perturbations induced by the clouds. Moreover, since most clouds in earth's atmosphere are produced by upward air motions, their vertical structure and distribution are direct markers of these motions: stronger, smaller horizontal-scale convective motions produce cumuloform clouds, whereas weaker, larger horizontal-scale synoptic motions produce stratiform clouds. So, one key piece of information for understanding cloud dynamical feedbacks is the cloud vertical structure (CVS) and its variations and how they relate to the atmospheric circulation on both weather and climate scales.

Until recently, the most extensive cloud datasets containing relevant information about CVS were those obtained from surface weather observations (Warren et al. 1986, 1988; Hahn et al. 1994, 1996, 2001), from weather satellites by the International Satellite Cloud Climatology Project (ISCCP; Rossow and Schiffer 1991, 1999), and inferred from radiosonde measurements of the vertical profiles of temperature and humidity (Poore et al. 1995; Wang and Rossow 1995; Wang et al. 2000). The surface observation dataset provides information from a ''bottom up'' viewpoint about the vertical distribution of cloud-base heights above local topography. Although statistics of the coincident occurrence of clouds at different levels within a region about 30–50 km across have

Corresponding author address: William B. Rossow, CREST at The City College of New York, Steinman Hall (T-107), 140th Street and Convent Avenue, New York, NY 10031.
E-mail: wbrossow@ccny.cuny.edu

DOI: 10.1175/2010JCLI3734.1

been compiled to describe CVS (Hahn et al. 1982, 1984, 2001; Warren et al. 1985), such a result requires ''overlap'' assumptions, since the surface observer only actually sees clouds at different levels in different parts of the sky. In other words, only the lowermost cloud base in each vertical column is actually viewed, and the statistics only provide direct information about the vertical *distribution* of clouds, not the cloud vertical *structure*. The coverage of this dataset (Warren et al. 1986, 1988) is not globally complete (Southern Ocean coverage being especially sparse) and does not provide information about synoptic variations over oceans.

The ISCCP dataset, which is globally complete and resolves mesoscale to synoptic-scale cloud variations (there are other satellite cloud products but, because they are based on polar-orbiting satellite observations, they have poorer time resolution), provides information from a ''top down'' viewpoint about the vertical distribution of cloud-top locations (like most other satellite products). Although information about the coincident occurrence of clouds at different levels within a region about 280 km across is available, overlap assumptions are again required to convert these to CVS. In other words, the satellite imagers and sounders only see the uppermost cloud top in each vertical column and the statistics only provide direct information about the vertical distribution of clouds, not the cloud vertical structure. A different, though limited, view of the structure of the uppermost cloud layers was provided by the Stratospheric Aerosol and Gas Experiment (SAGE) instrument (Liao et al. 1995a; Wang et al. 1996). The importance of the overlap assumptions to radiative heating is illustrated in Chen et al. (2000).

The radiosonde measurements of the vertical profile of relative humidity provide more direct information about CVS, not just the cloud vertical distribution, by identifying coincident saturated layers in the atmosphere; however, the coverage and sampling of this dataset is even sparser than the surface observation dataset. Nevertheless, to date this dataset (Wang et al. 2000) provides the only information about CVS that does not require overlap assumptions.

To calculate the vertical distribution and weather-scale variations of radiative heating for the ISCCP flux data based on D-series ISCCP data (FD) product (Zhang et al. 2004), we needed to develop a complete description of the CVS at 3 h, 300-km scale from this set of incomplete observations; thus, we combined the radiosonde and satellite (ISCCP) information into a statistical CVS model that provides global coverage (Rossow et al. 2005). The model is based on the plausible idea that CVS is related to the meteorology-like cloud types and that cloud types can be recognized by satellites (as shown by Lau and Crane 1995; Hahn et al. 2001). This model is statistical in the sense that it uses assumed relationships of cloud types and CVS that reconcile the monthly cloud layer distribution statistics from the two datasets as a function of latitude and season over land and ocean separately. Thus, the cloud layer distribution results are expected to be reasonably good. A similar analysis is possible with the radiosondes and surface observation dataset using the latter's classification of cloud types; however, in Rossow et al. (2005), the surface observations of low cloud amounts were used to check the CVS model. Further evaluation of this CVS model serves to provide error estimates for the vertical distribution of radiative flux divergences in the ISCCP-FD product, now being used in many studies; however, more importantly, such an evaluation advances understanding of the relationship between CVS and other cloud properties by testing the specific hypothesis underlying this model's construction.

The launch of *CloudSat* (radar) and CALIPSO (lidar) into the A-train constellation of satellites in 2006 provides the first direct CVS measurements with uniform and complete global coverage (Stephens et al. 2002; Winker et al. 2003, 2006). However, these instruments only view the nadir point along the track of their sun-synchronous polar orbits, providing only a diurnally aliased, two-dimensional slice through the clouds. Thus, these datasets still provide an incomplete view of cloud structure, lacking information about diurnal variations and about cloud system evolution (the time resolution is effectively 1 day). A statistical combination of the *CloudSat* and CALIPSO (C&C) data with a conventional satellite imager dataset, like that produced by the Moderate Resolution Imaging Spectroradiometer (MODIS) on *Aqua* in the A-train, can be used to estimate an instantaneous 3D view of clouds; however, to study the time evolution of the 3D structure of clouds, the C&C dataset has to be combined with the whole weather satellite constellation using the ISCCP dataset. As a first step toward this goal, we use an early version of the combined C&C cloud layer profiles to evaluate our previous statistical model of CVS. This study specifically tests the hypothesis that the cloud types defined by top pressure and optical thickness correspond to specific CVS; although originally based on the climatological statistics of cloud layer distributions, we pose the most severe test by matching individual satellite views and comparing the CVS found.

2. Datasets

The previous 3D cloud dataset was created from a climatology of CVS from radiosonde humidity profiles (Wang et al. 2000) and a climatology of cloud layer types from ISCCP (Rossow and Schiffer 1999) on an equal-area mapping equivalent to 2.5° latitude–longitude intervals at

the equator (in section 3 this dataset is referred to as ISCCP-FD CVS). Accounting for the top-down view of the satellites, as well as some limitations of both datasets regarding detection and/or identification of thin cirrus clouds, the cloud layer statistics of these two datasets could be reconciled by assigning specific CVS to specific combinations of cloud-top pressure and optical thickness based on the plausible assumption that increasing (total column) optical thickness corresponds to an increasing numbers of cloud layers: smaller optical thicknesses correspond to single-layer clouds, an intermediate range of optical thicknesses correspond to double-layer clouds, larger optical thicknesses correspond to three-layer clouds, and the largest optical thicknesses correspond to vertically extensive (physically thick) cloud layers (Rossow et al. 2005). Wang et al. (2000) showed that the majority of clouds exhibit a roughly constant physical layer thickness distribution independent of top height; however, there is a small population, interpreted to be deep convection, with layer thicknesses linearly proportional to cloud-top height. A similar result obtained from C&C is discussed by Mace et al. (2009). Using the ISCCP cloud-top pressure categories to define high (H), middle (M) and low (L) clouds, the CVS is classified in terms of single-layer clouds (called 1H, 1M, 1L), double-layer clouds (HL, HM, ML), and triple-layer clouds (HML), with a separate CVS type for deep convection, called HxMxL, which is a single extensive cloud layer from the boundary layer to the high troposphere. The specific optical thickness (τ) ranges are 1H ($\tau < 3.6$), HM ($3.6 < \tau < 9.4$), HML ($9.4 < \tau < 23$), HxMxL ($23 < \tau$), 1M ($\tau < 1.3$), and ML ($9.4 < \tau$). There is one special case where a middle cloud (according to ISCCP) with $1.3 < \tau < 9.4$ is changed to an HL structure (see Rossow et al. 2005). For comparison to the C&C results, we apply the same classification to individual satellite pixels from the ISCCP D-series pixel data (DX) dataset; this dataset is called the ISCCP-DX CVS.

The *CloudSat* cloud layer profiles are obtained from 94-GHz radar reflectivity profiles with 240-m vertical sampling intervals at 1.1-km spacing along the orbit ground track (700-m instantaneous field of view). Clouds are detected when their reflectivity exceeds a threshold, but there are some additional aspects of the algorithm employed to reduce the effects of radar noise (to increase detection sensitivity) and ground clutter (Marchand et al. 2008). These additional steps help mitigate the main limitations, which are detecting optically very thin clouds and clouds very close to the surface (tops below about 1 km). Basic cloud layer statistics from the first year of *CloudSat* data are reported in Mace et al. (2007, 2009); we use release 4.

The CALIPSO cloud profiles are obtained from two-channel (532- and 1064-nm wavelengths) polarized lidar reflectivity profiles with 30–60-m vertical sampling (in the troposphere) at 330-m spacing along the orbit ground track (70-m instantaneous field of view). Clouds are detected by reflectivities above the molecular scattering background (which is larger during daylight because of scattered sunlight), but there are additional algorithm procedures to reduce the effects of noise (to increase detection sensitivity; Vaughan et al. 2004). The main limitation of this dataset is that the lidar cannot penetrate clouds with visible optical thicknesses larger than about 3, so the vertical profile is incomplete below any thicker cloud layer. The lidar is much more sensitive to the presence of very optically thin clouds, but such clouds can also be confused with aerosols. There are specific algorithm procedures to separate these; however, in version 2 (Liu et al. 2004), which we use here, there is an excess of low-level clouds reported in areas dominated by low, broken clouds and some spurious cloud layers are reported below clouds that have attenuated the lidar (Hagihara et al. 2010). Version 3 of the CALIPSO products, which reduces these problems, has just been released. Basic cloud layer statistics from CALIPSO have been reported in Winker et al. (2006).

To obtain the best representation of CVS, a combined analysis of the radar and lidar has been developed by Mace et al. (2009). Essentially, a cloud is taken to be present in a specific layer if either instrument reports its presence. Since the lidar has smaller sampling intervals in both vertical and horizontal directions, a cloud fraction threshold is employed (50% of the lidar samples within the radar sample must be cloudy) to combine the profiles. We use the combined information in the level 2B cloud Geometrical Profile 2B-GEOPROF–lidar product, release 4, epoch 2. We convert cloud-top heights to cloud-top pressures using a climatological atmosphere based on Oort's compilation (Oort 1983). We call this dataset C&C in the remainder of the paper. There are some issues with this version of the C&C results. As already noted, the version 2 CALIPSO results appear to report too much low-level cloudiness, especially in areas of broken boundary layer clouds (Hagihara et al. 2010). In addition, there appears to be an algorithm problem that sometimes causes reports of clouds below the uppermost layer even though the lidar is fully attenuated (Hagihara et al. 2010). These two problems would tend to increase the amount of isolated low-level cloud and the amount of multilayer cloudiness. In contrast, the radar has difficulty detecting very low-lying clouds. Because the logic to combine the two results reports a cloud if either sensor detects a cloud, the *CloudSat* underestimate of low-level cloudiness is overcompensated for by CALIPSO for isolated low cloudiness and offset by some amount for low clouds under other clouds.

TABLE 1. Classification match and mismatch statistics (% of total) for one month (October 2006, about 18 million samples) of global data from C&C where C&C-self refers to C&C matches to C&C at separations of 25 km, and from ISCCP-DX CVS matched to C&C (about 45 million samples). Each individual pixel is classified as clear or one of three cloud-top pressure categories (L = PC > 680 mb, M = 680 < PC < 440 mb, and H = PC < 440 mb) based on the topmost cloud layer in each profile. See text for explanation of the last two sets of numbers.

C&C	Clear	High	Middle	Low	Total
C&C-self matched	14.6	37.2	6.0	22.5	80.3
Unmatched	5.9	3.9	3.1	6.8	19.7
Total	20.5	41.1	9.1	29.3	100
ISCCP-DX CVS matched	14.7	20.9	2.4	12.7	50.7
Unmatched	6.3	20.0	6.8	16.2	49.3
Total	21.0	40.9	9.2	28.9	100

3. CVS evaluation

a. CVS at pixel level

Because our ultimate goal is to combine the higher time-resolution ISCCP cloud product with the C&C product to obtain information about the variations of CVS at meteorological space–time scales, we conduct the severest test of our hypothesis by comparing the statistical CVS model applied to individual satellite pixels from the ISCCP-DX product (ISCCP-DX CVS) with individual space-collocated and time-coincident C&C profiles. Because the ISCCP CVS depends on cloud optical thickness, the comparison is for daytime only. Given the finer C&C spatial sampling along the orbit track (about 1 km), each ISCCP pixel is collocated on average with about 70 or so C&C pixels, all of which are included in our statistics. The C&C product combines many 70-m lidar fields of view with the 700-m radar field of view; each of these is collocated with an ISCCP DX pixel, which is about 5 km in size and sampled at about 25–30-km intervals every 3 h. The navigation accuracy of the ISCCP pixels is similar to the spacing interval. Thus, the differences in the spatial sampling in this comparison, due to mislocations and differing fields of view, are expected to cause an intrinsic amount of disagreement. Moreover, there is an additional sampling effect because of time differences (sample times can differ by up to 3 h).

The only available way to estimate the expected magnitude of disagreement because of the differences in spatial sampling is to collect statistics comparing C&C pixels separated by about 25 km to each other (referred to as C&C-self). A similar analysis was done with ISCCP compared with surface observations (Rossow et al. 1993). Note that this estimate has to be an underestimate, since the only effect evaluated is due to differing locations; the effects of differing fields of view and differing times are not included in this estimate. Hence, this test of our CVS model is very strict.

TABLE 2. Classification truth table (% of total) comparison of ISCCP-DX and C&C CVS for October 2006, adjusted for sampling noise and renormalized (cf. Table 1). The boldface numbers are for the matched CVS.

	C&C	Clear	High	Middle	Low	Total
ISCCP CVS	Clear	**18.3**	8.8	1.9	6.9	35.9
ISCCP CVS	High	0.5	**26.0**	1.4	2.3	30.2
ISCCP CVS	Middle	0.0	6.5	**3.0**	2.5	12.0
ISCCP CVS	Low	0.0	4.8	1.3	**15.8**	21.9
	Total	18.8	46.1	7.6	27.5	100

The first part of Table 1 shows the results of comparing C&C profiles to each other: each profile is classified as either H, M, or L by the pressure of the uppermost cloud layer top (see section 2) in each profile plus the clear category (four types). Table 1 also shows the comparison of C&C with the collocated ISCCP-DX CVS for the four types. To keep the language clear, we will always refer to the "true" state of a pixel in terms of its C&C classification and talk about "matched ISCCP" (i.e., the classifications agree) and "unmatched ISCCP" classifications for those pixels.

Almost all of the unmatched ISCCP pixels for C&C clear pixels and about half of the unmatched ISCCP cloudy pixels for C&C middle- or low-level clouds can be attributed to sampling errors (Table 1). Therefore, we adjust the "truth table" numbers to account (in part) for the sampling error by subtracting the C&C self-matched fraction in equal proportions from each of the ISCCP unmatched categories and then renormalizing the total to 100% to give the results shown in Table 2.

When C&C declares the pixel to be clear, the corresponding ISCCP pixels are almost always labeled clear (after accounting for sampling); however, on the rare occasions when ISCCP does detect clouds associated with C&C clear pixels (which might still be accounted for by the time sampling mismatch), they are generally isolated high-level clouds according to ISCCP. Such clouds are usually barely detected only in the IR but not the visible (VIS) and might be false detections. When C&C identifies high-level clouds (H), slightly less than half of the cases are mislabeled by ISCCP; however, almost half of these are labeled as clear sky, suggesting that this portion of the disagreement can be explained by the thin cirrus clouds that ISCCP does not detect (cf. Liao et al. 1995a; Jin et al. 1996; Stubenrauch et al. 1999): the underestimate of total cloud amount shown in Table 2 (about 17%) is about the same as found in the cited studies. C&C identifies middle-topped clouds only about two-thirds as frequently as ISCCP, a bias that has long been noted (cf. Rossow and Schiffer 1999). When C&C identifies middle-level clouds (M), fewer than half

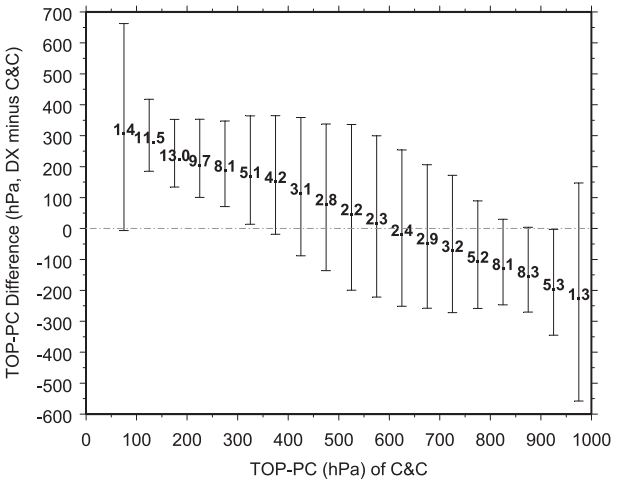

FIG. 1. Plot of average of the cloud-top pressure (PC in hPa) difference (DX minus C&C) for the topmost cloud layer as a function of C&C (both radar and lidar) PC values from October 2006. The standard deviations are indicated by the error bars, and the fraction of cases for each value is indicated by the numbers.

of the associated ISCCP pixels agree, although the ''matched fraction'' is about half of the C&C total and the largest of all categories with the ''unmatched fraction'' spread about equally among all of the alternatives. When C&C identifies low clouds (L), a surprisingly large fraction of corresponding ISCCP pixels are mislabeled (more than 40%), more than half of these are labeled as clear. This result is surprising because the ISCCP detection thresholds have been carefully evaluated for detection of low-level clouds, which can be difficult in the IR but is much easier in VIS (cf. Rossow et al. 1993; Rossow and Schiffer 1999), with little evidence of a significant bias. The alternate lidar analysis by Hagihara et al. (2010) greatly reduces this disagreement. The CALIPSO team also concluded that the version 2 CALIPSO product, which we use here, confuses aerosol with low-level cloud too often in low-cloud cases; therefore, they have reprocessed the product into version 3 to correct this effect. Thus, we interpret most of this portion of the disagreement as being caused by the CALIPSO overestimate of low cloud amounts.

In summary, if an account is taken of isolated thin cirrus clouds missed by ISCCP and an overestimate of low clouds by CALIPSO, then Table 2 shows that the largest disagreement between ISCCP and C&C CVS (four types) is for middle-topped clouds: about 15% of C&C high-topped clouds are mislabeled as middle-topped clouds by ISCCP. Overall, only a little more than half of the clouds are correctly classified as H, M, or L by ISCCP DX (but the space–time sampling effects are underestimated).

Some of the differences of CVS in Table 2 occur because differences of cloud-top pressure (PC) between the two datasets for the uppermost cloud layer alter the CVS classification. Previous studies have already diagnosed several causes for ISCCP errors in PC values. Even if the cloud-top temperature is correct, errors in the atmospheric temperature profile used to assign cloud-top pressure can redistribute the cloud layers: the temperature dataset used by ISCCP for this purpose tends to underestimate cloud-top pressures for low-level clouds, especially over oceans (Stubenrauch et al. 1999; Wang et al. 1999), and to overestimate cloud-top pressures for middle-level clouds (Stubenrauch et al. 1999). There is a systematic difference between the location of the physical cloud top, as detected especially by lidar, and the infrared emission top, which is located at an infrared optical thickness of about 1, well below the physical top; this causes an apparent overestimate of cloud-top pressures, especially for upper-level clouds in the tropics (Liao et al. 1995b; Wylie and Wang 1997). Correction for transmitted IR radiation when cloud optical thickness is very low (below about 1) tends to produce errors in cloud-top pressure of both signs (Luo and Rossow 2004). Finally, a thin cloud layer overlying another cloud layer tends to cause an overestimate of cloud-top pressure because the IR transmission of the uppermost layer is overestimated (Liao et al. 1995a; Jin and Rossow 1997). These errors do not necessarily change the H, M, L classification for all clouds, rather they bias the fraction of clouds in each category, causing a tendency to shift some clouds from H and L into M, as seen in Table 2.

Figure 1 shows an evaluation of these differences as the mean difference (standard deviation show by error bars) as a function of PC determined by C&C. Only pixels that are cloudy in both datasets are included, so there is no effect on these results from isolated thin cirrus layers missed by ISCCP or the extraneous low-level clouds from CALIPSO. The figure shows a monotonic variation of the average PC differences from about +300 hPa (ISCCP larger) for PC = 100 hPa to about −150 hPa for PC = 900 hPa. Comparing C&C with itself shows that about 50 hPa of the high bias in high cloud PC and about 50 hPa of the low bias in low cloud PC are associated with sampling effects. The reason that sampling produces a bias at either end of the range is that the distribution of PC differences is no longer symmetric near the extremes: more differences of one sign than the other are more likely near the limits. So, overall, there is about a 200-hPa high bias in ISCCP PC values at PC $<$ 300 hPa and a 50 hPa low bias at PC $>$ 800 hPa. These results are quantitatively consistent with the studies cited above.

Without any constraint on how well the PC values agree for collocated ISCCP and C&C pixels, only about 61% of the cloudy cases (about 1% more over ocean and 4% less over land) agree on the H, M, L identifications.

TABLE 3. As in Table 1, but for nine types of CVS (see text). Only cloudy pixels with the topmost cloud layer PC difference ≤150 mb are included, about half the total sample population used in Tables 1 and 2. The nine CVS types are identified directly for C&C and are based on the statistical model for ISCCP, where the vertical structure depends on cloud-top pressure (of the topmost layer seen by satellite) and the total column TAU. The results have been adjusted as in Table 2. The boldface numbers are for the matched CVS.

C&C	Clear	1H	HM	HML	HxMxL	HL	1M	ML	1L	Total
					ISCCP					
Clear	**30.7**	6.1	0.0	0.0	0.6	2.8	2.6	0.0	13.2	56.0
1H	1.1	**5.1**	0.0	0.0	0.0	0.0	0.0	0.0	0.0	6.2
HM	0.0	0.0	**0.4**	0.0	0.0	0.0	0.0	0.0	0.0	0.4
HML	1.0	0.0	0.0	**0.2**	2.1	0.0	0.0	0.0	0.0	3.3
HxMxL	0.0	0.0	0.0	0.0	**3.3**	0.0	0.0	0.0	0.0	3.3
HL	0.3	0.0	0.0	0.1	0.0	**0.3**	1.6	0.0	0.0	2.3
1M	0.0	0.0	0.0	0.0	0.0	0.0	**0.3**	0.0	0.0	0.3
ML	1.1	0.0	0.0	0.0	0.6	0.0	2.6	**0.6**	0.3	5.2
1L	1.0	0.0	0.0	0.0	0.0	0.0	0.0	0.0	**22.0**	23.0
Total	35.2	11.2	0.4	0.3	6.6	3.1	7.1	0.6	35.5	100

Accounting for sampling effects (approximate but underestimated) increases the agreement on H, M, L identifications to about 70%. To test the hypothesis relating PC–TAU cloud types to unique CVS more clearly, we separate out the errors due to erroneous top-pressure classification by applying a constraint on the magnitude of the PC difference. The fraction of cloudy pixels that agree increases monotonically as the PC difference is constrained to smaller values while the total number of matched pixels decreases. If the PC difference is not allowed to exceed 150 hPa, the agreement on top height categories (H, M, L) increases to about 85% (a few percent less over land); at least 5% of this disagreement is still explained by sampling error (estimated from C&C-self).

Note that, although the top-pressure classification is constrained to agree better, this does not guarantee agreement for the full CVS (nine types), as there is no constraint on cloud layers below the topmost layer. With no constraints or corrections for sampling effects, only about 35% of the both cloudy cases (4% more over oceans and 9% less over land) agree on the full CVS; correcting for sampling effects and constraining the PC difference to <150 hPa increases the matched fraction to about 53% (3% more over oceans but 16% less over land) with about half of the matched cloudy pixels discarded. Table 3 shows the comparison of the full ISCCP-DX CVS (nine types) compared with C&C with a correction for sampling (same procedure as applied to Table 2) and the difference of the topmost cloud layer PC ≤150 hPa.

Table 3 shows that almost all of the C&C clouds labeled clear by ISCCP are categorized by C&C as either 1H or 1L; the latter is assumed to be caused by the CALIPSO analysis flaw in version 2, and the former

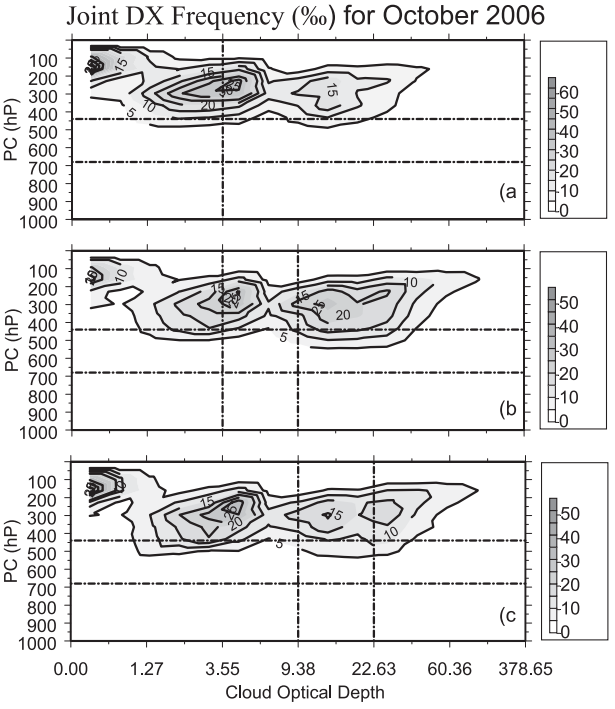

FIG. 2. Joint histograms of ISCCP cloud-top pressure (PC in hPa) and TAU for all collocated C&C profiles that are classified as (a) 1H, (b) HM, and (c) HML. Results are for all matched cloudy pixels over the globe where the PC difference of the uppermost cloud layer is ≤150 hPa.

confirms that the extra C&C high clouds are cirrus that are too thin for ISCCP to detect (they cannot be thin cirrus placed at the wrong level, because there is no cloud layer below according to C&C). There is also a small fraction of C&C 1M and HL cases, but these may still be sampling effects. The relative proportion of the missed 1H clouds is quantitatively consistent with previous estimates of the amount of cirrus missed by ISCCP (Jin et al. 1996; Stubenrauch et al. 1999). The presence of very thin cirrus clouds overlying other clouds can be mislabeled by ISCCP (Jin and Rossow 1997); however, the CVS model attempts to correct for this by assigning some midlevel clouds to the HL category (Rossow et al. 2005), with only partial success as we will show.

To explain further the relationship between the ISCCP-DX CVS (nine types) and the C&C profiles, we sort the ISCCP observations into joint distributions of PC and optical thickness (TAU) for each CVS category as identified by C&C. Figure 2 shows the results for three of the high-topped categories (1H, HM, and HML) that are separated in the ISCCP CVS by particular ranges of TAU (the dashed lines in these figures indicate the PC and TAU ranges correspond to the ISCCP CVS). The three peaks in the distribution are produced by small discontinuities in the ISCCP ice cloud lookup table but are mainly due to

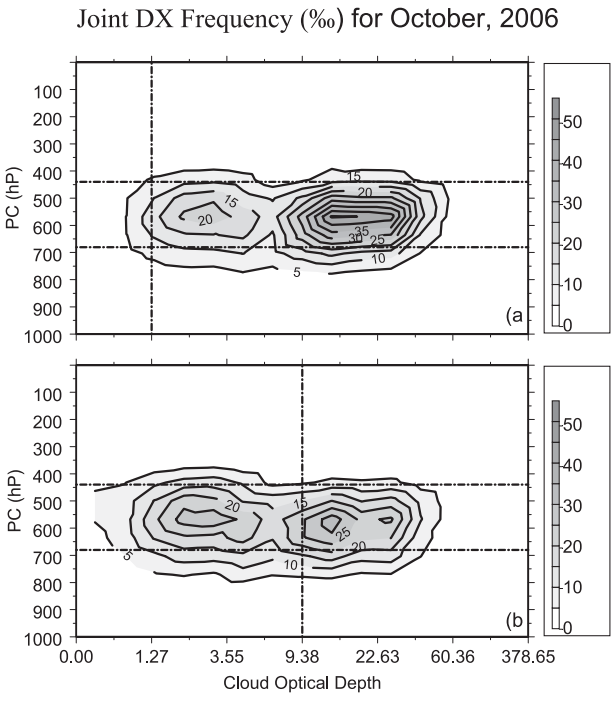

FIG. 3. As in Fig. 2, but classified as (a) 1M and (b) ML. Results are for all matched cloudy pixels over the globe where the PC difference of the uppermost cloud layer is ≤150 hPa.

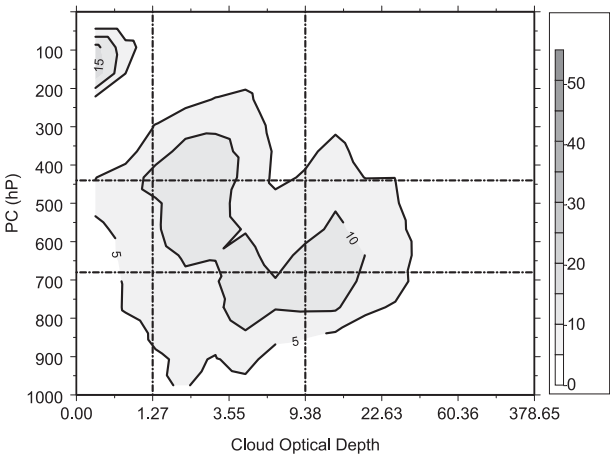

FIG. 4. As in Fig. 3, but for HL. Results are for all matched cloudy pixels over the globe, without any constraint on the PC difference of the uppermost cloud layer.

the low precision of the histograms shown. The figure shows that all three CVS categories have qualitatively similar PC–TAU distributions, but there is some tendency for a shift of the centroid of TAU values among the three cases. Although the 1H category has its peak frequency at the smallest TAU values, as assumed in the CVS model, there are significant occurrences at moderate TAU values up to about 6. The ISCCP CVS assumes that TAU for HM is smaller than for HML, whereas Fig. 2 shows that HML is globally more concentrated at moderate values than HM. In the tropics there is no significant difference in the distributions of TAU for these two categories. As Table 3 shows, the ISCCP CVS spreads the HM category between HML (because of the reversed relation with TAU), HL, ML, and even 1L, the latter two results suggesting that the total optical thickness for thin cirrus overlying middle-level clouds can have smaller total TAU values than assumed in the ISCCP CVS model. Similarly, the HML category is also spread among these categories. HxMxL (not shown) is correctly associated with the largest TAU values.

Figure 3 shows the PC–TAU distributions for the C&C categories 1M and ML. There is again a tendency to reverse the TAU values associated with these two categories, with 1M being more concentrated at larger values instead of the very small values assumed in the ISCCP CVS. The ML case exhibits a nearly uniform TAU distribution from 1 to 30. Figure 4 shows the PC–TAU distribution without a PC constraint for the C&C HL category. The constraint is removed in this figure to see how well the ISCCP CVS reassigns an originally middle-topped case to an HL case: most of the TAU values are in the middle range (indicated by dashed lines), and the ISCCP PC values indicate middle-level clouds. In this TAU range, the ISCCP CVS reassigns these clouds to the HL category. Table 3 shows that the attempt to correct for the cloud-top location error that ISCCP makes when a thin cirrus overlies a low-level cloud has shifted the results in the right direction, producing more frequent matches with the C&C HL category (sampling error accounts for most of the unmatched cases); however, most of these cases are still assigned to 1M.

Taking account of sampling effects, cloud detection differences and the difference between the physical and radiative cloud top, the pixel matchup results confirm the basic accuracy of the ISCCP PC values and show good agreement for the basic cloud layer height categories. The attempt to classify each height category further into specific CVS using TAU ranges to identify multilayer situations shows some agreement for the high-cloud categories and some success correcting apparently middle-level clouds to the HL category. Although there is a tendency for the TAU ranges associated with 1H, HM, HML, and HxMxL to increase, as assumed in the ISCCP CVS, the separation of these categories is not strong, and there is more of tendency for HML to be optically thinner than HM. The high-cloud results might be improved a little using the following categories: 1H ($\tau < 2.4$), HML ($2.4 < \tau < 6.3$), HM ($6.3 < \tau < 23$), and HxMxL ($23 < \tau$).

The assumed TAU ranges for 1M and ML appear to be the opposite of what occurs and there does not appear to be any real distinction in TAU between the ML and HL

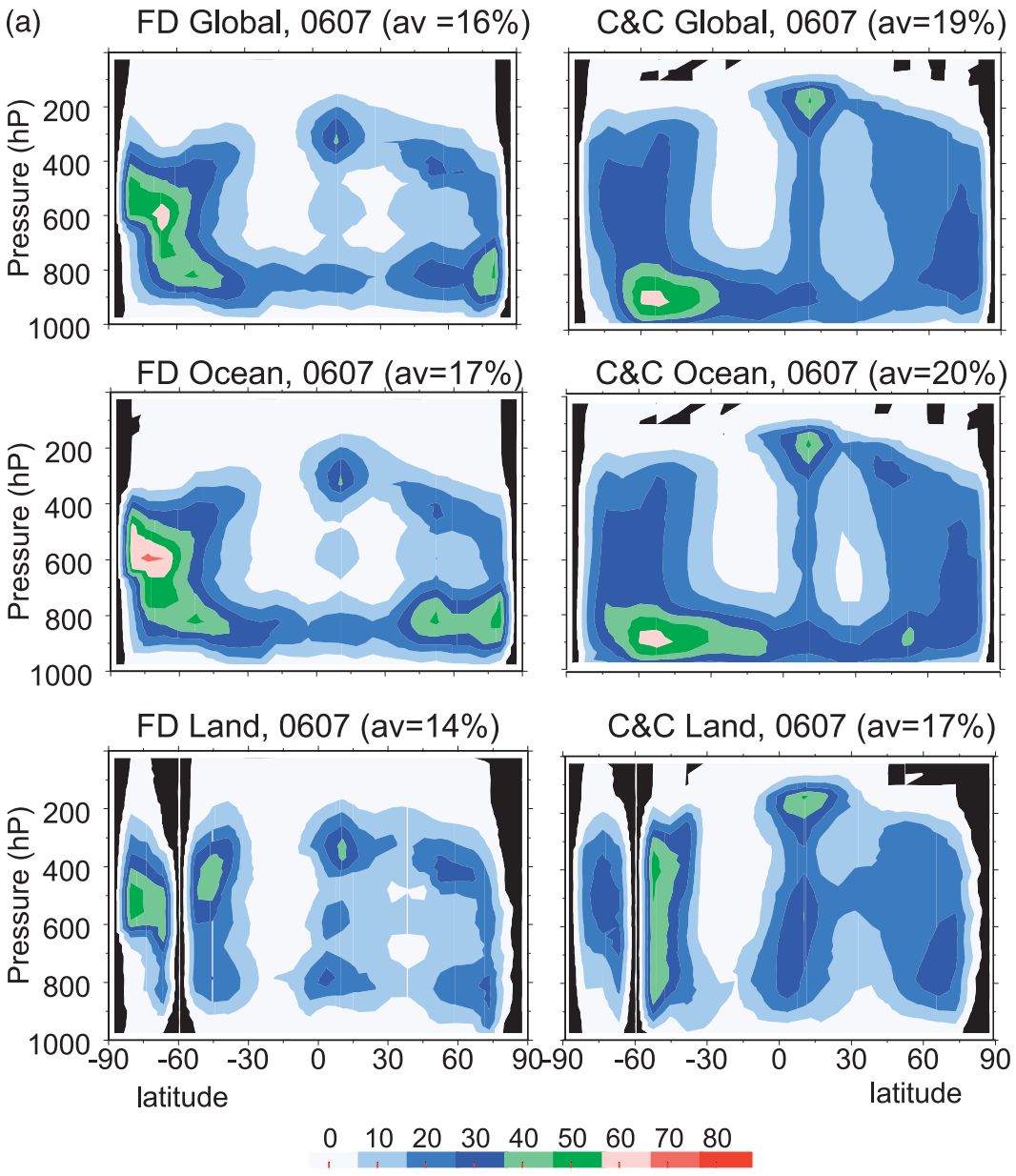

FIG. 5. Pressure–latitude cross sections of the zonal monthly-mean cloud amounts (in %) for (a) July 2006 and (b) January 2007: (left) ISCCP-FD CVS, (right) C&C CVS, (top) global results, (middle) averaged only over oceans, and (bottom) averaged only over land. Black color is for undefined values.

cases. Results might be improved slightly using the following categories: HL ($\tau < 2.4$), ML ($2.4 < \tau$ 9.4) and 1M ($9.4 < \tau$). Here the separation by TAU ranges is poor.

b. *Statistical CVS*

Since the ISCCP CVS was developed as a statistical fit to observations of the vertical distribution of clouds, the average distribution of cloud layers may still exhibit good agreement with the C&C results, even though the pixel matchup CVS agreement is poorer. This can be the case especially when the categories are not cleanly separated but do correspond to observed tendencies, as we have found in the high-level cloud cases at least. Note also that, without any constraint of the PC of the uppermost cloud layer, ISCCP misidentifies a little more than half of the middle-topped clouds and misplaces only about one-seventh of the high clouds into the middle category, and that the total cloud fraction involved in these errors is less than 10% (Table 2); thus, the disagreement discussed for middle-topped clouds contributes only a small part of the

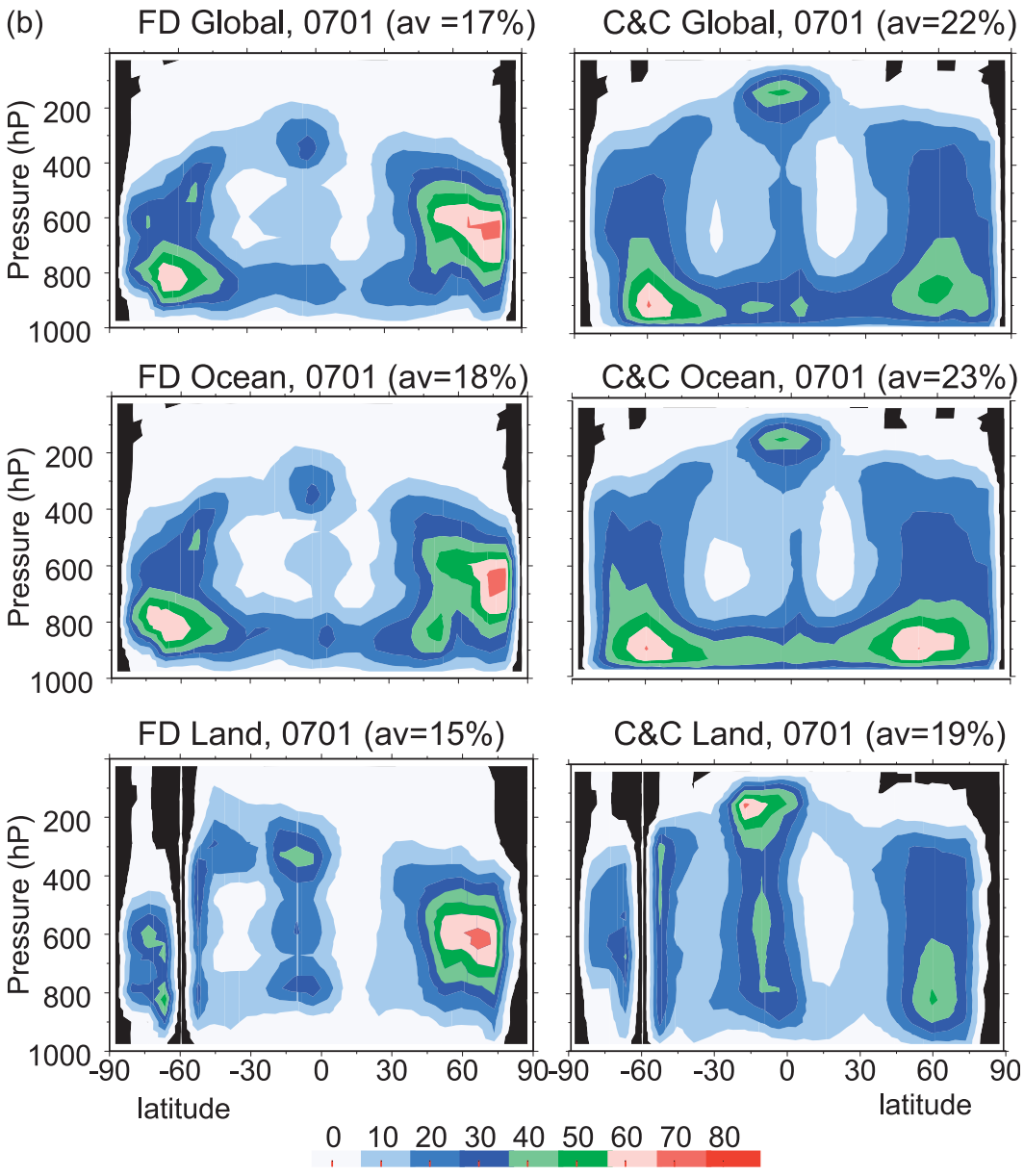

FIG. 5. (*Continued*)

story. Moreover, as Table 3 shows, when we remove the effect of the misplacement of the uppermost cloud top (and of sampling), there is only about 10% cloud fraction that appears in the HL, 1M, and ML categories for both ISCCP and C&C. To show that the statistical agreement is better than the individual pixel matchup, we compare in Fig. 5 the monthly, zonal mean cross sections of cloud layer amounts based on the ISCCP-FD CVS (earlier results were for the CVS model applied to individual pixels in the ISCCP-DX dataset; these results are from the ISCCP-FD dataset based on ISCCP-D1 data) with the results compiled from C&C for July 2006 and January 2007 for the whole globe and separately for land and ocean areas. The results are compiled at 5° intervals because this grid resolution produces more uniform sampling statistics for the sparse C&C data.

In Fig. 5 both datasets show similar large-scale cloud layer distribution features that are indicative of the atmospheric general circulation: 1) a tropical and two midlatitude storm zones marked by higher total cloud amounts with vertically extensive cloud distributions; 2) two zones between the tropics and midlatitudes

relatively free of clouds at all levels, especially over land and except for a concentration of low-level clouds over the ocean; 3) seasonal excursions of the latitude of the ITCZ, which tends to produce a subtropical zone exceptionally clear of clouds in the winter hemisphere, and of the Northern Hemisphere cyclones (northward in boreal summer), but not of the Southern Hemisphere cyclones; and 4) a seasonal variation of vertical extent in midlatitudes (upward in local winter).

Rossow et al. (2005) drew attention to a number of other specific features of the ISCCP CVS cross sections based on a 3-yr average. The features that are confirmed by C&C are 1) a broader ITCZ over land in January than in July; 2) a narrower ITCZ over ocean in July (the hint of a double feature in January is not seen in the ISCCP data in Fig. 5, which is based only on single months of data); 3) a triple vertical peak structure in the ITCZ, not seen in Fig. 8 in Mace et al. (2009), which shows only an annual-mean cross section; 4) a subtropical minimum of clouds at all levels over land; 5) a subtropical concentration of low clouds over ocean; 6) in the Northern Hemisphere midlatitudes, a single broad vertical distribution of clouds in wintertime but a double-peaked distribution in summertime; and 7) Antarctic clouds with larger vertical extent in wintertime.

Features that are not confirmed by C&C are 1) in the Southern Hemisphere midlatitudes, a single broad vertical distribution year round but with lower vertical extent in summertime; and 2) Arctic clouds with a larger vertical extent in summertime. Two other features that are not confirmed by C&C are 1) greater amounts of upper-level clouds in southern midlatitudes than northern midlatitudes, which is not apparent in the single-month ISCCP results in Fig. 5 either (the ISCCP results in the figure are consistent with the C&C results in showing a seasonal variation with more upper-level clouds in the summer hemisphere); and 2) a larger vertical extent of summertime clouds over northern midlatitude land areas than over oceans that is not as apparent in C&C.

Other global features noted in Rossow et al. (2005) include 1) a general decrease of high-level cloud amounts from lower to higher latitudes, confirmed by C&C; 2) a general increase of middle- and low-level clouds with latitude, which ISCCP exaggerates for middle-level clouds in the winter hemisphere and underestimates for low-level clouds in the Southern Hemisphere over oceans; 3) a general deficit of middle-level clouds relative to low- and high-level clouds, except in the polar regions, which C&C confirms but the midlevel polar cloudiness is overestimated by ISCCP, especially in wintertime; 4) a general deficit of high- and low-level clouds over tropical land areas relative to oceans, which may have been a particular feature of the 3-yr-averaged results because the ISCCP results in Fig. 5 show more high-level clouds over land than ocean in agreement with C&C; 5) a general increase of high-level cloud amounts over midlatitude land areas relative to oceans in summertime, which is not apparent in either the ISCCP and C&C results in Fig. 5; and 6) much larger low-level cloud amounts over subtropical and midlatitude oceans than over adjacent land areas, which C&C confirms.

Two other differences between the ISCCP-FD and C&C CVS that can be seen in Fig. 5 are 1) an underestimate by ISCCP of low-level clouds over Southern Hemisphere midlatitude oceans, especially in wintertime, is partly a misplacement of these clouds to a higher level; and 2) midlatitude cloudiness more concentrated toward low levels instead of midlevels in C&C than ISCCP FD, especially in winter.

Figure 6 makes the main differences between the ISCCP-FD and C&C CVS clearer by showing the zonal monthly-mean cloud amount anomaly differences as a function of latitude and pressure for July 2006 and January 2007. To reduce the effect of cloud detection differences, each dataset in Fig. 5 is first normalized to its own total cloud amount by converting the values at each pressure-latitude to an anomaly relative to the average over its own cross section, then differences are formed for Fig. 6. The largest differences highlight the general underestimate by the ISCCP of cloud amounts at the highest levels, above the 200-hPa level, especially in the tropics, and an overestimate of middle-level cloudiness in the winter polar regions, poleward of about 60°. The former difference is associated with the tendency of the infrared-based cloud tops to lie below the lidar cloud tops as well as the missed very thin cirrus in the ISCCP results (cf. Wylie and Wang 1997). The latter difference was noted in Rossow et al. (2005), where the odd results might be explained by the fact that the radiosonde humidity sensor is not really working very well at the cold temperatures encountered in the upper atmosphere in the polar regions; this explanation is reinforced by the fact that the discrepancy is larger in polar winter than summer. Smaller differences show an underestimate of middle-level clouds over tropical land areas and an underestimate of low-level cloudiness in southern high midlatitudes over ocean. The vertical misplacement of ISCCP low-level cloudiness over oceans is caused by the particular atmospheric temperature profile used by the ISCCP to convert cloud-top temperatures to pressures (cf. Wang et al. 1999); the fact that this causes a larger difference in the Southern than Northern Hemisphere may arise because of the dominance of Northern Hemisphere radiosonde observations used to test the atmospheric temperature retrieval and employed in the ISCCP CVS statistical model. Overall, the rms differences are $<10\%$.

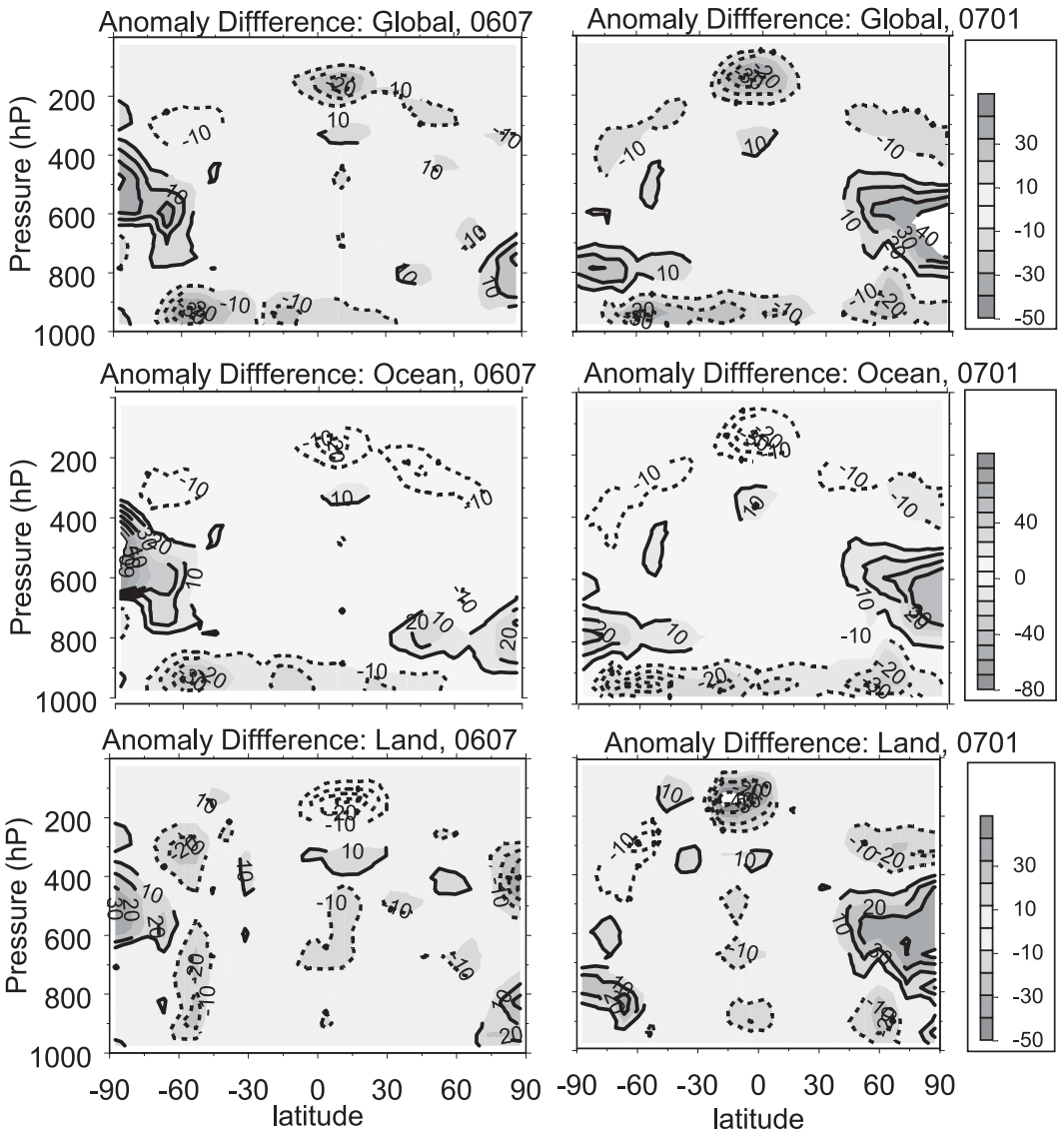

FIG. 6. Pressure–latitude cross sections of the differences (ISCCP FD minus C&C) of the zonal monthly-mean cloud amount anomalies (in %), where the anomalies are first determined relative to the average over the cross section for each dataset: (left) results for July 2006, (right) results for January 2007, (top) global results, (middle) averaged only over oceans, and (bottom) averaged only over land.

4. Discussion

The ISCCP CVS is crude but still produces a good statistical representation of the vertical distribution of cloud (the original basis of its design), in that rms differences of zonal monthly-mean cloud layer amounts (when normalized to the same total cloud amount as C&C) are generally $<10\%$ for most locations and levels. The most notable differences are the overestimate of the amount of middle-level cloudiness in the winter polar regions, which was also noted by Rossow et al. (2005) as the largest problem, and an underestimate of low-level cloudiness over southern midlatitude oceans. The systematic difference in cloud tops, especially in the tropics, is partly a difference of definition of cloud top, partly the effect of the lidar's better sensitivity to the presence of very thin cirrus, and partly a result of the intrinsic limitation of imager determinations of the location of optically thinner cloud tops when they overlie lower-level clouds. Only the latter error has a significant radiative effect (Chen et al. 2000).

We have conducted a much more severe test of the CVS model here. The basic idea of assigning a vertical-layer number based on the total cloud (column) optical thickness seems to work reasonably well for situations

where the uppermost cloud layer is a high-level cloud (and, of course, for isolated low-level clouds): the assumed increase in layer number with increasing optical thickness is seen as a statistical tendency; however, the distinction between different categories is not sharp, and there is a suggestion that the relative optical thickness of HM and HML should be reversed. This assumption was not successful for situations where the uppermost cloud layer is a middle-level cloud (only a small subset of all clouds), even though the attempt in the ISCCP-FD CVS to correct for the mislabeling of the high–low cases as middle-topped cases did move the results in the right direction. In fact, the C&C composites of optical thickness seem to indicate a tendency for 1M to have a larger (column) optical thickness than ML. Although the ISCCP-FD CVS did improve the statistics concerning low-level clouds, there still seems to be an underestimate of low cloud amount over Southern Hemisphere oceans, particularly at latitudes poleward of 50°S, which might be caused by the dominance of Northern Hemisphere humidity profiles in the radiosonde statistics.

Although we can now compile a much better idea of the geographic and seasonal variations of the average vertical distribution of clouds from C&C—a statistical 3D description—we cannot study the time evolution of CVS for individual cloud systems given the severe limitations of the space–time sampling of the C&C observations; these measurements are diurnally aliased to two times of day and limited to nadir track views. To study the time evolution of CVS, we will need to combine the C&C observations with those from ISCCP (the only cloud dataset with diurnal time resolution) in some statistical fashion. One method is to improve the identification of different layer distributions from imaging data, such as ISCCP, as we did before, replacing the radiosonde profiles with those from C&C. Some results, particularly those in the polar regions, will be much improved by using C&C with ISCCP. Although the high clouds seem classifiable by TAU ranges, the middle-level clouds seem much more problematic. Although a different set of TAU ranges may improve the results a little, it appears that more information about the meteorological situation is needed to better separate the cases. In particular, it may not be physically sensible to expect a separation of cloud layer categories at the scale of individual satellite pixels (≈1–5 km); rather the classification might work better when applied at a larger, meteorologically (dynamically) relevant spatial scales.

Acknowledgments. We thank Hajime Okamoto and Yuichiro Hagihara for their discussion of these results and their lidar analysis. We also acknowledge useful conversations with Kaori Sato, Jay Mace, and Dave Winker. This work was supported by the NASA *CloudSat*/CALIPSO program (H. Maring), NASA Grant NNXD7AT10G; and the NASA MEASURES program (M. Maiden), NASA Grant NNDXD8AL79A.

REFERENCES

Chen, T., Y. Zhang, and W. B. Rossow, 2000: Sensitivity of radiative heating rate profiles to variations of cloud layer overlap. *J. Climate,* **13,** 2941–2959.

Hagihara, Y., H. Okamoto, and R. Yoshida, 2010: Development of a combined CloudSat-CALIPSO cloud mask to show global cloud distribution. *J. Geophys. Res.,* **115,** D00H33 doi:10.1029/2009JD012344.

Hahn, C. J., S. G. Warren, J. London, R. M. Chervin, and R. L. Jenne, 1982: Atlas of simultaneous occurrence of definite cloud types over oceans. NCAR Tech. Note NCAR/TN-201+STR, 29 pp. [Available from Data Support Section, National Center for Atmospheric Research, Boulder, CO 80307.]

——, ——, ——, ——, and ——, 1984: Atlas of simultaneous occurrence of definite cloud types over land. NCAR Tech. Note NCAR/TN-241+STR, 42 pp. [Available from Data Support Section, National Center for Atmospheric Research, Boulder, CO 80307.]

——, ——, and ——, 1994: Climatological data for clouds over the globe from surface observations, 1982-1991: Total cloud edition. CDIAC Tech. Rep. NDP026A, 42 pp. [Available from Carbon Dioxide Information Analysis Center, Oak Ridge National Laboratory, Oak Ridge, TN 37831.]

——, ——, and ——, 1996: Edited synoptic cloud reports from ships and land stations over the globe, 1982-1991. CDIAC Tech. Rep. NDP026B, 45 pp. [Available from Carbon Dioxide Information Analysis Center, Oak Ridge National Laboratory, Oak Ridge, TN 37831.]

——, W. B. Rossow, and S. G. Warren, 2001: ISCCP cloud properties associated with standard cloud types identified in individual surface observations. *J. Climate,* **14,** 11–28.

Jin, Y., and W. B. Rossow, 1997: Detection of cirrus overlapping low-level clouds. *J. Geophys. Res.,* **102,** 1727–1737.

——, ——, and D. P. Wylie, 1996: Comparison of the climatologies of high-level clouds from HIRS and ISCCP. *J. Climate,* **9,** 2850–2879.

Lau, N.-C., and M. W. Crane, 1995: A satellite view of the synoptic-scale organization of cloud properties in midlatitude and tropical circulation systems. *Mon. Wea. Rev.,* **123,** 1984–2006.

Liao, X., W. B. Rossow, and D. Rind, 1995a: Comparison between SAGE II and ISCCP high-level clouds 1. Global and zonal mean cloud amounts. *J. Geophys. Res.,* **100,** 1121–1135.

——, ——, and ——, 1995b: Comparison between SAGE II and ISCCP high-level clouds 2. Locating cloud tops. *J. Geophys. Res.,* **100,** 1137–1147.

Liu, Z., M. Vaughan, D. Winker, C. Hostetler, L. Poole, D. Hlavka, W. Hart, and M. McGill, 2004: Use of probability distribution functions for discriminating between cloud and aerosol in lidar backscatter data. *J. Geophys. Res.,* **109,** D15202, doi:10.1029/2004JD004732.

Luo, Z., and W. B. Rossow, 2004: Characterizing tropical cirrus life cycle, evolution, and interaction with upper-tropospheric water vapor using Lagrangian trajectory analysis of satellite observations. *J. Climate,* **17,** 4541–4563.

Mace, G. G., R. Marchand, Q. Zhang, and G. L. Stephens, 2007: Global hydrometeor occurrence as observed by CloudSat:

Initial observations from summer 2006. *Geophys. Res. Lett.,* **34,** L09808, doi:10.1029/2006GL029017.

——, Q. Zhang, M. Vaughan, R. Marchand, G. Stephens, C. Trepte, and D. Winker, 2009: A description of hydrometeor layer occurrence statistics derived from the first year of merged Cloudsat and CALIPSO data. *J. Geophys. Res.,* **114,** D00A26, doi:10.1029/2007JD009755.

Marchand, R. T., G. G. Mace, T. Ackerman, and G. Stephens, 2008: Hydrometeor detection using *CloudSat*—An earth-orbiting 94-GHz cloud radar. *J. Atmos. Oceanic Technol.,* **25,** 519–533.

Oort, A. H., 1983: Global atmospheric circulation statistics, 1958-1973. NOAA Prof. Paper 14, 180 pp.

Poore, K. D., J. Wang, and W. B. Rossow, 1995: Cloud layer thicknesses from a combination of surface and upper-air observations. *J. Climate,* **8,** 550–568.

Rind, D., and W. B. Rossow, 1984: The effects of physical processes on the Hadley circulation. *J. Atmos. Sci.,* **41,** 479–507.

Rossow, W. B., and R. A. Schiffer, 1991: ISCCP cloud data products. *Bull. Amer. Meteor. Soc.,* **72,** 2–20.

——, and ——, 1999: Advances in understanding clouds from ISCCP. *Bull. Amer. Meteor. Soc.,* **80,** 2261–2287.

——, A. W. Walker, and L. C. Garder, 1993: Comparison of ISCCP and other cloud amounts. *J. Climate,* **6,** 2394–2418.

——, Y.-C. Zhang, and J.-H. Wang, 2005: A statistical model of cloud vertical structure based on reconciling cloud layer amounts inferred from satellites and radiosonde humidity profiles. *J. Climate,* **18,** 3587–3605.

Stephens, G. L., and Coauthors, 2002: The CloudSat mission and the A-train: A new dimension of space-based observations of clouds and precipitation. *Bull. Amer. Meteor. Soc.,* **83,** 1771–1790.

Stubenrauch, C. J., W. B. Rossow, F. Chéruy, A. Chédin, and N. A. Scott, 1999: Clouds as seen by satellite sounders (3I) and imagers (ISCCP). Part I: Evaluation of cloud parameters. *J. Climate,* **12,** 2189–2213.

Vaughan, M. A., S. A. Young, D. M. Winker, K. A. Powell, A. H. Omar, Z. Liu, Y. Hu, and C. A. Hostetler, 2004: Fully automated analysis of space-based lidar data: An overview of the CALIPSO retrieval algorithms and data products. *Laser Radar Techniques for Atmospheric Sensing,* U. N. Singh, Ed., International Society for Optical Engineering (SPIE Proceedings, Vol. 5575), 16–30.

Wang, J., and W. B. Rossow, 1995: Determination of cloud vertical structure from upper-air observations. *J. Appl. Meteor.,* **34,** 2243–2258.

——, ——, T. Uttal, and M. Rozendaal, 1999: Variability of cloud vertical structure during ASTEX observed from a combination of rawinsonde, radar, ceilometer, and satellite data. *Mon. Wea. Rev.,* **127,** 2484–2502.

——, ——, and Y. Zhang, 2000: Cloud vertical structure and its variations from a 20-yr global rawinsonde dataset. *J. Climate,* **13,** 3041–3056.

Wang, P.-H., P. Minnis, M. P. McCormick, G. S. Kent, and K. M. Skeens, 1996: A 6-year climatology of cloud occurrence frequency from Stratospheric Aerosol and Gas Experiment II observations (1985–1990). *J. Geophys. Res.,* **101,** 29 407–29 429.

Warren, S. G., C. J. Hahn, and J. London, 1985: Simultaneous occurrence of different cloud types. *J. Climate Appl. Meteor.,* **24,** 658–667.

——, ——, ——, R. M. Chervin, and R. L. Jenne, 1986: Global distribution of total cloud cover and cloud type amounts over land. NCAR Tech. Note NCAR/TN-273+STR, 229 pp. [Available from Data Support Section, National Center for Atmospheric Research, Boulder, CO 80307.]

——, ——, ——, ——, and ——, 1988: Global distribution of total cloud cover and cloud type amounts over the ocean. NCAR Tech. Note NCAR/TN-317+STR, 212 pp. [Available from Data Support Section, National Center for Atmospheric Research, Boulder, CO 80307].

Winker, D. M., J. R. Pelon, and M. P. McCormick, 2003: The CALIPSO mission: Spaceborne lidar for observation of aerosols and clouds. *Lidar Remote Sensing for Industry and Environment Monitoring III,* U. N. Singh, T. Itabe, and Z. Liu, Eds., International Society for Optical Engineering (SPIE Proceedings, Vol. 4893), 1–11.

——, M. Vaughan, and B. Hunt, 2006: The CALIPSO mission and initial results from CALIOP. *Lidar Remote Sensing for Environmental Monitoring VII,* U. N. Singh, T. Itabe, and D. Narayana Rao, Eds., International Society for Optical Engineering (SPIE Proceedings, Vol. 6409), 640902.

Wylie, D. P., and P.-H. Wang, 1997: Comparison of cloud frequency data from the high-resolution infrared radiometer sounder and the Stratospheric Aerosol and Gas Experiment II. *J. Geophys. Res.,* **102,** 29 893–29 900.

Zhang, Y., W. B. Rossow, A. A. Lacis, V. Oinas, and M. I. Mishchenko, 2004: Calculation of radiative fluxes from the surface to top of atmosphere based on ISCCP and other global data sets: Refinements of the radiative transfer model and the input data. *J. Geophys. Res.,* **109,** D19105, doi:10.1029/2003JD004457.